Journal of Superconductivity and Novel Magnetism (2021) 34:3377–3383
https://doi.org/10.1007/s10948-021-06024-4

ORIGINAL PAPER

Microstructure Evolution of Ni-Co Alloys During Crystallization and Amorphization Process

Yong-chao Liang[1] · Rui-bo Ma[1] · Li-li Zhou[2] · Mu He[3] · Ze-an Tian[1,4] · Yun-fei Mo[5]

Received: 5 July 2021 / Accepted: 31 August 2021 / Published online: 10 September 2021

Abstract
A molecular dynamics simulation has been conducted in $Ni_{73}Co_{27}$ and $Ni_{74}Co_{26}$ alloys during rapid solidification at the cooling rate of 1×10^{12} K/s. It indicates that two phase transitions occur with twice drops, and the number of FCC increases suddenly in $Ni_{73}Co_{27}$ alloy. And finally, FCC atoms are dominant with the amount of 92.94% at 300 K, which neatly arranges themselves into the crystalline structure. A lot of topologically close-packed clusters are formed in $Ni_{74}Co_{26}$ alloy, indicating the formation of metallic glass. The differences between the formations in crystalline hexagon and amorphous pentagon are demonstrated by three-dimensional visualization.

Keywords Molecular dynamics simulation · Ni-Co alloys · Crystal structures · Amorphous structures

1 Introduction

Because amorphous materials have high strength mechanical properties and excellent corrosion resistance and chemical compatibility [1], and crystal materials have unique structural characteristics and excellent physical and chemical properties [2], both of them have been attracted much attention in the field of materials science. Meanwhile, the variation of the microstructure during crystallization and amorphization phase transformation will cause the change of physical properties [3]. Therefore, crystallization and amorphization phase transformation have been the subject of a considerable significance in both theoretical and experimental work.

✉ Yong-chao Liang
20113248@qq.com

1 School of Big Data and Information Engineering, Guizhou University, Guiyang 550025, China

2 Department of Information Engineering, Gannan Medical University, Ganzhou 341000, China

3 The Herbert Wertheim College of Engineering, University of Florida, Gainesville, FL 32609, USA

4 College of Computer Science and Electronic Engineering, Hunan University, Changsha 410082, China

5 School of Electronic and Communication Engineering, Changsha University, Changsha 410003, China

It is found that there are many factors affecting crystallization and amorphization phase transformation. For example, the amorphous structures are formed at the cooling rates of 1×10^{13} and 1×10^{12} K/s in $Cu_{10}Ag_{90}$ alloy, and the crystallized structures are formed when the cooling rate is lower than 1×10^{11} K/s, and the degree of crystallization increases with decreasing cooling rate [4]. It has been performed to simulate ion-beam-induced epitaxial crystallization and interfacial amorphization at an amorphous/crystalline Si interface, and a divacancy and di-interstitial pair can induce amorphization and crystallization [5]. $Ti_{50}Al_{45}Si_5$ multicomponent powders which are synthesized by mechanical alloying and heat treatment [6, 7] can present an amorphous phase or crystallization phase due to the degree of mechanical alloying and micro-structural properties [8]. Taking pure copper as an example, crystal nucleation occurs due to the emergence of adequate crystal-like clusters, while glass formation in some critical cooing rate region is determined by atomic structural fluctuation [9].

In addition to above factors, composition on crystallization and amorphization in alloys are also important. For example, the minor addition of Nb can improve the glass-forming ability by shortening the start time of the amorphization reaction in $Zr_{66.7-x}Cu_{33.3}Nb_x$ alloys, and the amorphous $Zr_{66.7}Cu_{33.3}$ phase gradually transforms into a metastable FCC-Zr_2Cu phase [10]. The amorphous phase appears in Fe-50Ti, and the amorphous phase is formed directly and at much lower energies in Fe-33.3Ti system

during mechanical alloying of Fe-xTi ($x = 33.3$ and 50 at.%) alloys [11]. The crystallization and amorphous transition are observed in different components of Fe–Ni alloys during the isothermal relaxation process [12]. Therefore, the alloy composition not only is important for crystallization and amorphization, but also has an impact on material properties. Currently, Ni-Co alloys, as a representative of transition-metal, are widely studied for their unique properties such as strong adsorption [13, 14]; however, there is no analysis in crystallization and amorphization on the atomic scale. In addition, due to the limitations of even the most advanced experimental techniques, there is still a lack of detailed understanding of the microstructure evolution. Therefore, a computational simulation has been performed for studying the crystallization and amorphization in Ni-Co alloy. In this paper, the crystallization and amorphization are studied in $Ni_{73}Co_{27}$ and $Ni_{74}Co_{26}$ alloys during the rapid solidification process through molecular dynamics (MD) simulation.

2 Simulation Details

In this paper, MD simulation is performed using the large-scale atomic/molecular massively parallel simulator (LAMMPS) [15]. The 10,000 atoms of $Ni_xCo_{(100-x)}$ ($x = 73$, 74) alloys are randomly placed in individual cubic boxes. According to a periodic boundary condition, the time step for the system operation is set at 10^{-15} s. In the fixed *NPT* ensemble [16], the interaction potential between the atoms is indicated by an embedded-atom model (EAM) developed and optimized by G. P. Pun and Y. Mishin [17]. The relevant analog computation starts at 1800 K that is much higher than the experimental melting temperature ($T_m \sim 1500$ K) [18]. At first, a uniform initial velocity obey is a Gaussian distribution is assigned to all atoms in the system, and the system is isothermally relaxed for 1,000,000 steps at the initial temperature to enter the equilibrium state. Secondly, the system temperature is rapidly reduced to 300 K at the cooling rate of 1×10^{12} K/s, and they are recorded with an interval of 10 K to acquire the microcosmic information, including the spatial coordinates, atomic numbers, and atomic potential energy of all atoms in the system, which is used to explore microstructure evolution at different temperatures during the rapid cooling process. At last, the structural configuration and formation and evolutionary law of microstructures are deeply investigated by pair distribution function ($g(r)$ or PDF) curve [19], the energy-temperature (E-T) curve, Largest Standard Cluster Analysis (LSCA) [20], three-dimensional (3D) visualization [21], and tracking method. And the crystallization and amorphization are studied between $Ni_{73}Co_{27}$ and $Ni_{74}Co_{26}$ alloys under the same solidification conditions on microstructure.

3 Results and Discussion

3.1 Pair Distribution Function

In materials science, the pair distribution function is extensively used to research the distinguishing features of the microstructure owing to its objectivity and reliability, which can refer to the spherical shell within a certain distance of an appointed atom and the probability of other atoms appearing in this range. Figure 1 shows the $g(r)$ curves of ten $Ni_xCo_{(100-x)}$ alloys at 300 K. The first peak of $Ni_{73}Co_{27}$ alloy is higher than that of $Ni_{74}Co_{26}$ alloy, which indicates that the order degree of the first neighbor atoms is stronger in $Ni_{73}Co_{27}$ alloy. There is a new peak between the first and second main peaks in $Ni_{73}Co_{27}$ alloy, which indicates that the crystal nucleus has been formed [22]. However, the second peak splits into two sub-peaks in $Ni_{74}Co_{26}$ alloy, where the intensity of the left sub-peak is slightly greater than that of the right sub-peak, indicating the formation of an amorphous structure [23]. When the Ni content (C_{Ni}) ≤ 73, there are many sharp peaks in the $g(r)$ curves, and long-range ordered crystal structures are formed in the system. When $C_{Ni} \geq 74$, the second peak of $g(r)$ curve splits, which indicates that amorphous structures are formed. In order to study the formation process of crystallization and amorphization in Ni-Co alloys, two critical $Ni_{73}Co_{27}$ and $Ni_{74}Co_{26}$ alloys are selected as research objects.

3.2 Evolution of Energy

The average potential energy (APE), as a simple and effective method, can objectively show the preliminary characteristic of phase transition by tracing the thermal

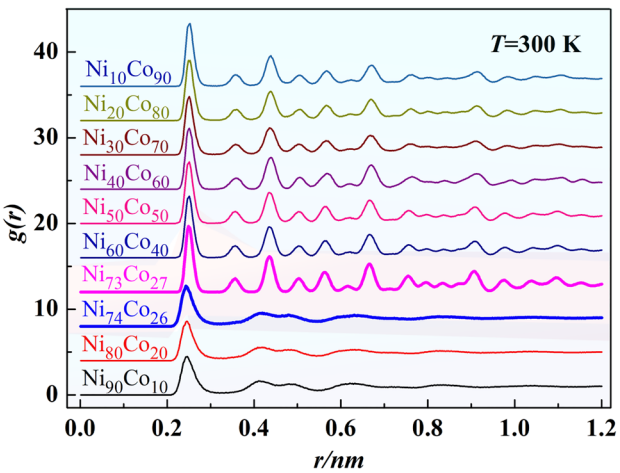

Fig. 1 The $g(r)$ curves of $Ni_xCo_{(100-x)}$ alloys at 300 K

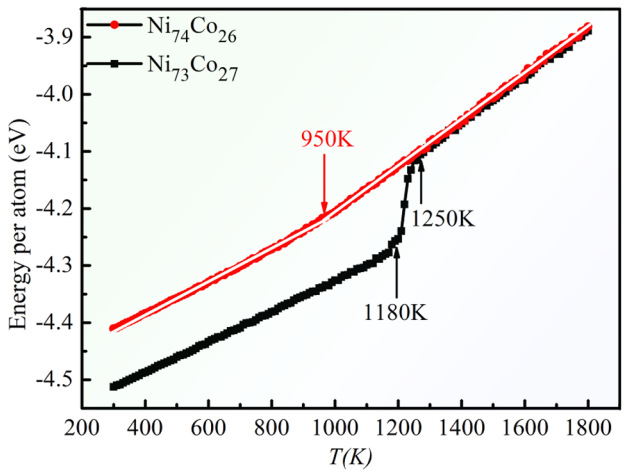

Fig. 2 Average potential energy of $Ni_{73}Co_{27}$ and $Ni_{74}Co_{26}$ alloys evolves with T

history in material science. As shown in Fig. 2, it can be seen that the APEs of two alloys decrease with the decrease of temperature. And the APEs are almost coincident at a temperature within the range of 1800 to 1250 K, which indicates that the difference of APE is not obvious in areas of elevated temperatures. The APE of $Ni_{73}Co_{27}$ suddenly drops at 1250 K, which is thought to be the crystallization temperature [24]. And the second drop occurs at 1180 K, which undergoes a second-order phase transition. The APE curve suddenly dropped, which indicates that a crystalline system should be formed. But the APE of $Ni_{74}Co_{26}$ gently declines without sudden change, so hence amorphous structures should be formed. When the slope of *E-T* curve changes, the temperature T at intersection can be regarded as the glass transition temperature Tg [25], which is about 950 K. In addition, the APE of $Ni_{74}Co_{26}$ is slightly higher than that of $Ni_{73}Co_{27}$ at 300 K, which indicates that the final structure of crystalline system is more stable than that of the amorphous system.

3.3 Bond-Type Index Analysis

The bond-type index analysis can clearly reflect the geometric characteristics of short-range atom arrangement. It can clearly show the bonding between atoms and neighboring atoms (see the inset in Fig. 3). In general, using the bond index method to analyze the structure, S421, S422, S444, and S666 are related to crystalline structures, whereas S555, S544, and S433 [26] are associated with amorphous structures. As shown in Fig. 3(a), the number of S421 changed most obviously during the rapid solidification in $Ni_{73}Co_{27}$ alloy. Its proportion is 3.6% at 1800 K, and suddenly increases to 72.84% at 1250 K, and then, it increases to 83.72% for the second time at 1180 K. At $T < 1180$ K, the amount of S421 increases slowly to 96.2% at last. On the contrary, the number of other bond types begins to decrease suddenly at 1250 K, and decrease steadily after 1180 K. The total number of other bond types accounted for only 5.85% at 300 K. Finally, the main crystalline structures composed of S421 are formed in $Ni_{73}Co_{27}$ alloy. As shown in Fig. 3(b), the number of S555 changes most obviously during the rapid solidification in $Ni_{74}Co_{26}$ alloy. Its proportion is 23.57% at 1800 K, and increases to 34.57% at 950 K, and finally reaches to 33.17% at 300 K. In addition, the numbers of S544 and S433 maintain at about 15% during the cooling process. The total number of three amorphous bond types ranges from 58.7% in initial liquid state to 64.44% in final amorphous state.

3.4 The Largest Standard Cluster Analysis

Although bond-type index analysis can be successfully used to describe the bonding relationship between an atom and its nearest neighbors, it still cannot describe the different basic clusters formed by an atom with its nearest neighbors [27]. Therefore, the LSCA method based on CTIM [28] is selected in this study to analyze the microstructure of the system [20]. The biggest advantage of this analysis method is that it can automatically confirm the unique cutoff distance

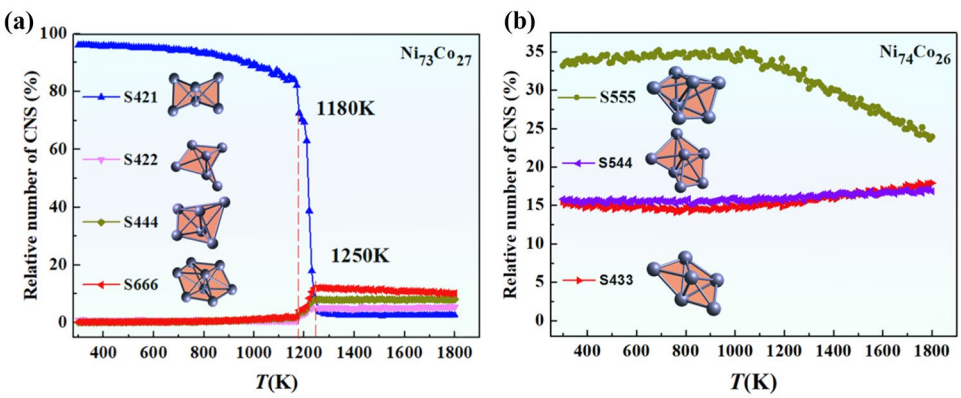

Fig. 3 Relative numbers of the main CNSs in $Ni_{73}Co_{27}$ and $Ni_{74}Co_{26}$ alloys

r_c [29], which indicates that the local structure characteristics of each atom can be uniquely and completely identified and characterized, so that it can objectively describe the local structure formed by each atom and its neighbor atoms in the system. The face-centered cubic structure (FCC) and hexagonal close-packed structure (HCP) LSCs are respectively denoted by [12/S421] and [6/S421, 6/S422] (see the inset in Fig. 4(a)) in crystalline structure.

At the same time, topologically close-packed (TCP) LSCs [30] are a group of LSCs that can be denoted as [n_4/S444, n_5/S555, n_6/S666] with $n_5 > 0$. Based on the Euler theorem, an equation set of $\{n_4 + n_5 + n_6 = CN, 2n_4 + n_5 = 12\}$ is satisfied for TCP LSCs. TCP structures are ubiquitous in liquid and metallic glass [31]. Therefore, the topological feature of a TCP LSC can be described by a TCP index of "*Ln*", where "*L*" is Z, A, B, C, D, or E, indicating $n_4 = 0, 1, 2, 3, 4, 5$; and *n* refers to *CN*. For example, typical TCP LSC of [12/S555] is Z12, i.e., icosahedron (ICO); a familiar TCP LSC of [1/S444, 10/S555, 2/S666] is A13 (see the inset in Fig. 4(b)) in amorphous structure.

As shown in Fig. 4(a), the number of FCC changes most obviously during the rapid solidification in $Ni_{73}Co_{27}$ alloy. The proportion of FCC is 0 at 1800 K, and suddenly increases to 58.98% at 1250 K, and then, it increases to 71.46% for the second time at 1180 K, corresponding to the second increase of energy. The amount of FCC increases slowly to 92.91% after 1180 K, and the system finally forms a standard FCC crystal structure. As shown in Fig. 4(b), there are different types of amorphous clusters in $Ni_{74}Co_{26}$ alloy, which are composed of amorphous bonds. Seven types of TCP structures are formed in Top10, and the number of amorphous clusters changes slightly. The amorphous clusters increase slowly at $T > T_g$, and the number of A13 changes most obviously. Its proportion 0.62% at 1800 K increases to 2.74% at 950 K. The growth of amorphous clusters is starting to flatten at $T < T_g$. The number floating of amorphous clusters is in consequence of unstable thermal fluctuation. In summary, only one crystal structure FCC influences structural characteristics during the crystallization process in $Ni_{73}Co_{27}$ alloy, but a variety of complex structures are formed during the amorphization process in $Ni_{74}Co_{26}$ alloy.

3.5 Topologically Close-Packed Analysis

TCP cluster phase with the lower average potential energy inhibits the growth and formation of crystals because of the interconnections between crystal and TCP clusters [4]. Therefore, TCP can reflect the degree amorphous of the system. As shown in Fig. 5, the number of TCP in two alloys is almost coincident in liquid state at $T > T_c$. At the beginning of T_c, the number of TCP in $Ni_{73}Co_{27}$ alloy suddenly decreases from 1555 to 36 at final, indicating that the degree of amorphization decreases and crystalline structures are formed. The number of TCP in $Ni_{74}Co_{26}$ alloy suddenly increases to 2051 at T_g, and then keeps a steady state. The evolution of TCP can demonstrate the beginning of crystallization and amorphization, which characterizes the local structure characteristics of amorphous structures.

3.6 Three-dimensional Visualization Analysis

It is necessary to delve into the formation of local structures at the atomic level. With the help of 3D visualization, the details of structural evolution can be intuitively presented. As shown in Fig. 6 (a), the central atom number of FCC, HCP, and BCC clusters in Ni73Co27 alloy suddenly

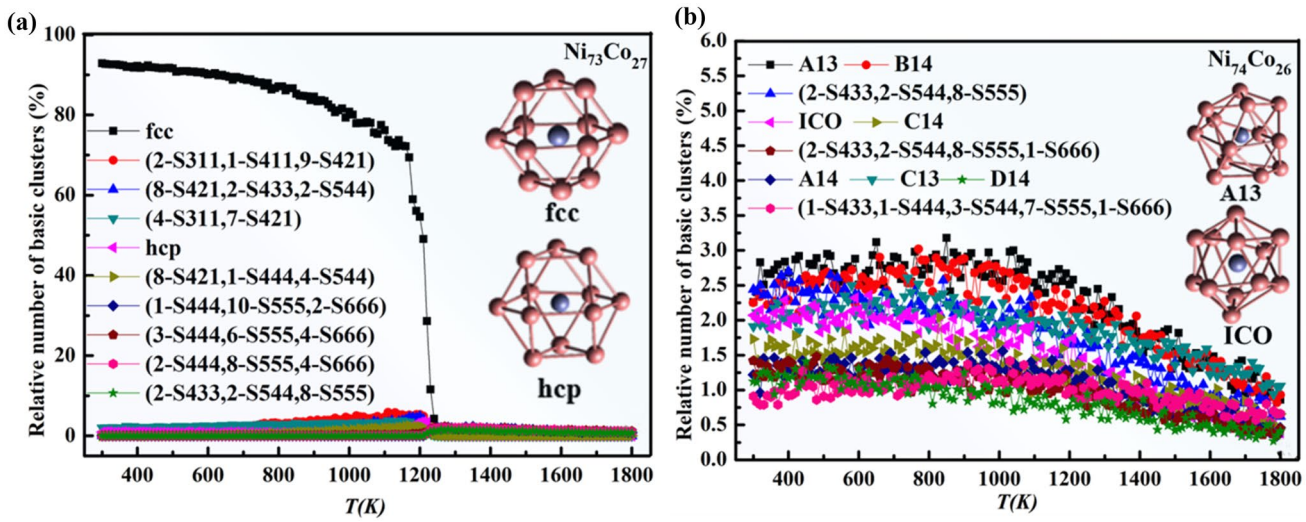

Fig. 4 Relative number of basic clusters in $Ni_{73}Co_{27}$ and $Ni_{74}Co_{26}$ alloys

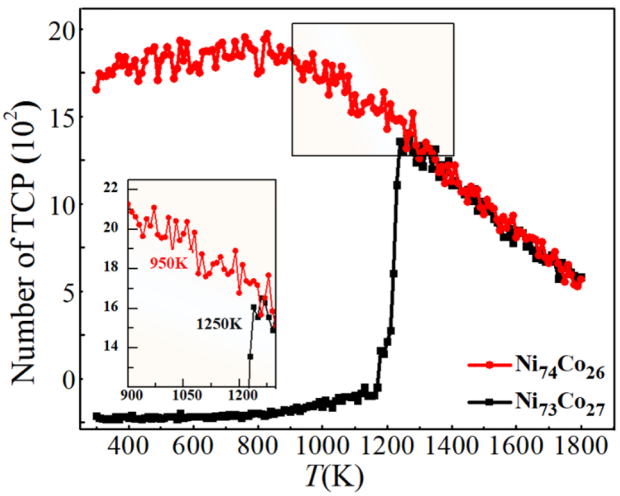

Fig. 5 The numbers of the TCP in $Ni_{73}Co_{27}$ and $Ni_{74}Co_{26}$ alloys

increases from 200 at 1250 K to 3216 at 1220 K, and then suddenly increases from 6179 at 1180 K to 7426 at 1100 K for the second time. The atomic arrangement becomes more and more regular with a drop in temperature. The second-order phase transformation leads to an increase in the degree of long-range order. When the number of atoms is 9394 (FCC: 9294, HCP: 99, BCC: 1) at 300 K, the near-perfect crystal structure with FCC ratio of 92.94% is formed at final. According to our previous research [12], the HCP atoms on the planar grain boundaries between FCC grains in $Ni_{73}Co_{27}$ are easy to be converted to FCC atoms at 1180 K, which results in a solid–solid phase transition, and more stable state, even a single-phase FCC crystal. The central atoms of the main TCP clusters are shown in Fig. 6(b) in $Ni_{74}Co_{26}$ alloy, such as A13, B14, C13, ICO, A14, C14, and D14. Compared with the crystal structure, the distribution of atoms is irregular, and the number of TCP increases slowly. The number of TCP increases from 705 at 950 K to 781 at 900 K, and remains a steady amount at $T < 900$ K, indicating that the amorphous structures change a little after T_g. Above all, it can be concluded that atomic proportions of Ni-Co alloys have a significant influence on microstructure during solidification. Even if the Ni atoms of two Ni-Co alloys differ by only 1%, it can cause the system to be crystallization or amorphization, and finally form crystal and amorphous structures.

3.7 The Evolution of Crystal and Amorphous Microstructures

From Fig. 4(a), it can be seen that FCC is the main crystal cluster type in the system; therefore, FCC is selected for further investigation in this study. FCC clusters in $Ni_{73}Co_{27}$ alloy are further investigated by the tracking method, as shown in Fig. 7. An FCC nano-cluster composed of 28 atoms (Fig. 7(a)) with 4 central atoms (Fig. 7 (d)) at 1270 K grows to be an FCC nano-cluster composed of 41 atoms (Fig. 7(b)) with 5 central atoms (Fig. 7 (e)) at 1260 K, and it becomes an FCC nano-cluster composed of 65 atoms (Fig. 7(c)) with 6 central atoms (Fig. 7(f)) at 1250 K. It reveals that the growing FCC nano-clusters are always distributed regularly, and the growth pathway of the nano-FCC clusters is shown in Fig. 7(g)–(i). The FCC with central atom 1893 (Fig. 7(g)) grows an FCC nano-clusters (Fig. 7(h)) by attaching 14 green atoms and 1 orange atom, and atoms 2038, 7555, 8106, 8980, 7059, and 6096 form a hexagonal structure with central atom 8092 through another hexagonal structure with central atom 1465, which form two new FCC clusters by intercross-sharing connection. Then, atoms 8092 and 9842 are bonded at 1250 K (Fig. 7(i)), and finally, one new FCC nano-cluster with 1893–1465-8092–9842 as the central atom is formed, in which atoms 8207, 8236, 9799, 7375, 6239, and 9002 form a hexagonal structure with central atom 9842. The symmetry of hexagon satisfies the basic symmetry characteristics of crystal structure, so it is determined that the crystal growth pathway is hexagonal nucleation in $Ni_{73}Co_{27}$ alloy.

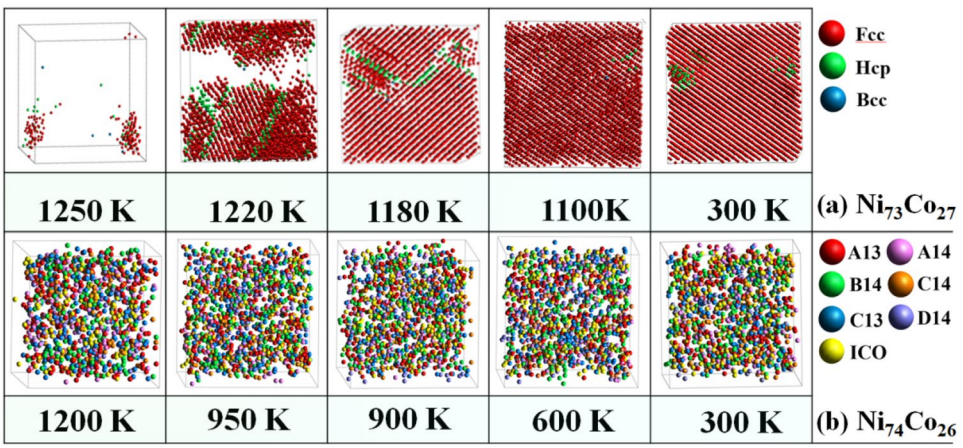

Fig. 6 Atomic distribution of two alloys near the phase transition temperature

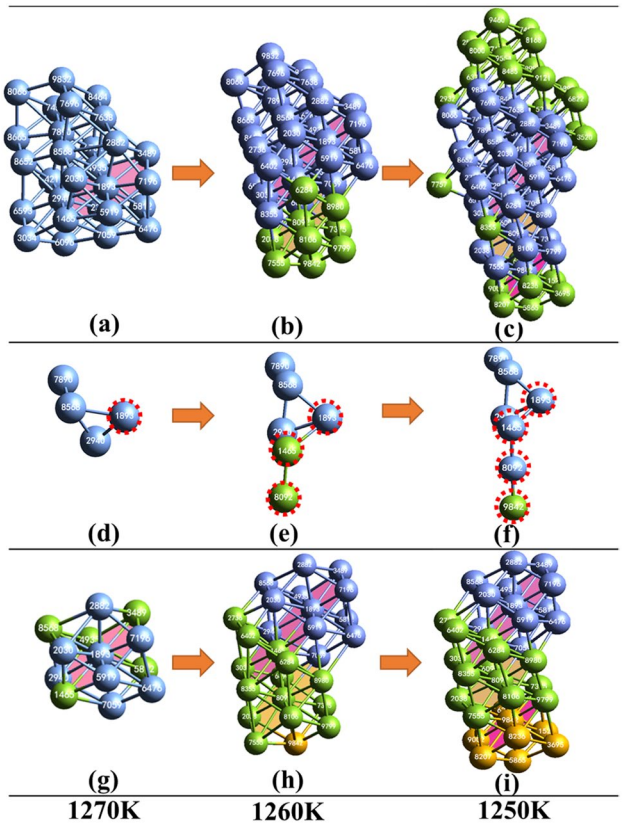

Fig. 7 The evolution of FCC at 1270–1250 K in $Ni_{73}Co_{27}$ alloy. (Blue and green-orange balls represent inherited and newly formed atoms, respectively)

Crystal and amorphous structures are different in the growth pathway. At present, the growth process of icosahedron has been tracked in amorphous MgZn alloys by the molecular dynamics method [32]. It is found that one icosahedron can grow to be nano-cluster by attaching a 6-atom pentagonal pyramid. TCP clusters with more complex than icosahedron in $Ni_{74}Co_{26}$ are further investigated by tracking method from 1270 to 1250 K, as shown in Fig. 8. A TCP nano-cluster composed of 37 atoms (Fig. 8(a)) at 1270 K with 4 central atoms (Fig. 8(d)) grows to be a new TCP nano-cluster composed of 42 atoms (Fig. 8(b)) with 5 central atoms (Fig. 8(e)) at 1260 K, and it becomes a TCP nano-cluster composed of 53 atoms (Fig. 8(c)) with 6 central atoms (Fig. 8(f)) at 1250 K. It reveals that the growing TCP clusters are always distributed in no regular arrangement, and demonstrates the growth pathway of TCP clusters as shown in Fig. 8(g)–(i). Central atoms 365 and 9041 of TCP clusters (Fig. 8(g)) are bonded at 1270 K to form a new TCP (Fig. 8(h)) by intercross-sharing connection, and atoms 9992, 9502, 5702, 2372, and 5467 form a pentagonal structure relating to a fivefold symmetry S555 with central atom 9041. And the location of atoms at 1260 K is different from that at 1270 K due to the motion of atoms. Then, central

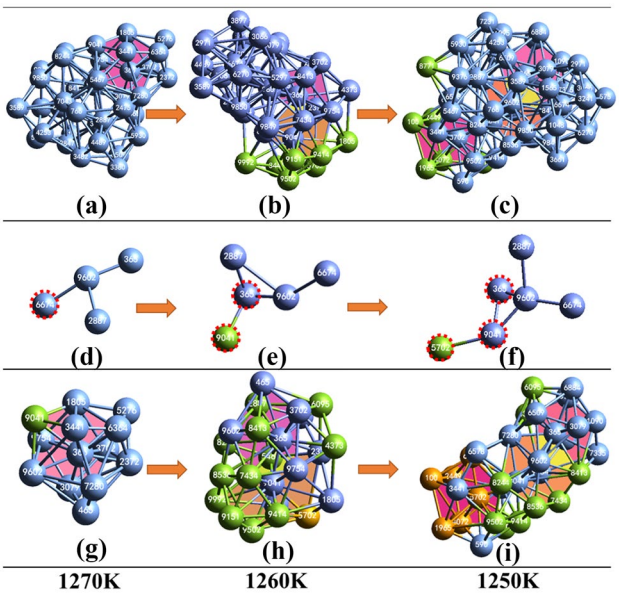

Fig. 8 The evolution of TCP at 1270–1250 K in $Ni_{74}Co_{26}$ alloy. (Blue and green balls represent inherited and newly formed atoms, respectively)

atoms 9041 and 5702 of TCP clusters (Fig. 8(i)) are bonded at 1250 K, and finally, an TCP nano-cluster with 365–9041-5702 as the central atoms is formed. Atoms 100, 1965, 9502, 9041, and 6364 form a pentagonal structure with central atom 5702, in which atoms 9414 and 5702 form a fivefold symmetry S555. The fivefold symmetry satisfies the basic characteristics of amorphous structure, so it is determined that the amorphous growth pathway is pentagonal formation through the necessary bond type such as S555 [33].

4 Conclusions

The microstructure evolutions have been systematically studied during crystallization and amorphization processes in $Ni_{73}Co_{27}$ and $Ni_{74}Co_{26}$ alloys by employing classical MD simulation. The following conclusions are obtained.

(1) The average potential energy of $Ni_{73}Co_{27}$ alloy suddenly drops at T_c, and the second drop occurs at 1180 K, which undergoes a second-order phase transition. The average potential energy of $Ni_{74}Co_{26}$ alloy declines without sudden change, so hence amorphous structures have been formed.

(2) S421 is the most obvious bond type in $Ni_{73}Co_{27}$ alloy, which suddenly increases twice, and the system finally forms a standard FCC crystal structure. S555 is the most obvious bond type in $Ni_{74}Co_{26}$ alloy, and the number of TCP clusters keeps a steady state after T_g, which

finally forming amorphous structure with a variety of complex structures.

(3) By the tracking method, the sixfold symmetry satisfies the characteristics of crystal structure, so the hexagonal nucleation is the growth pathway in $Ni_{73}Co_{27}$ alloy. While the fivefold symmetry satisfies the characteristics of amorphous structure, so the pentagonal formation is the growth pathway in $Ni_{74}Co_{26}$ alloy.

Funding This work has been supported by the National Natural Science Foundation of China (Grant Nos. 11964005, 11764005 and 12004053).

Data Availability The data that support the findings of this study are available from the corresponding author upon reasonable request.

References

1. Schuh, C.A., Hufnagel, T.C., Ramamurty, U.: Mechanical behavior of amorphous alloys. Acta Materialia. (2007).
2. Tang, X.F., Shi, S.Q., Fu, M.W.: Interactive effect of grain size and crystal structure on deformation behavior in progressive micro-scaled deformation of metallic materials. Intern. J. Machine Tools Manufact. 148:103473 (2019)
3. Geist, D., Ii, S., Tsuchiya, K., et al.: Nanocrystalline Zr_3Al made through amorphization by repeated cold rolling and followed by crystallization. J. Alloy. Compd. **509**(5), 1815–1818 (2010)
4. Zhang, D.E., Zhou, L.L., Liang, Y.C., et al.: Study on topologically close-packed and crystal clusters of $Cu_{10}Ag_{90}$ alloy at the critical crystalline cooling rate. CrystEngComm **22**, 7888–7895 (2020)
5. Motooka, T.: Molecular dynamics simulations for amorphous/crystalline Si interface: amorphization and crystallization induced by simple defects. Nuclear Instruments Methods Physic. Res. Sect. B: Beam Interact. Mater. Atoms. s127–128(none):244–247 (1997)
6. Velmurugan, C., Senthilkumar, V.: The effect of Cu addition on the morphological, structural and mechanical characteristics of nanocrystalline NiTi shape memory alloys. J. Alloy. Compd. **767**, 944–954 (2018)
7. Hasan, K.: Thermal stability, phase transformation and hardness of mechanically alloyed nanocrystalline $Fe_{-18}Cr_{-8}Ni$ stainless steel with Zr and Y_2O_3 additions. J. Alloys Comp. An Interdisciplin. J. Mater. Sci. Solid State Chem. Phys. (2018)
8. Jhla, B., Hkp, A., Jhj, A., et al.: Amorphization/crystallization behaviors of $Ti_{50}Al_{45}Si_5$ multi-component powder treated by mechanical alloying and subsequent heat treatment. J. Alloy. Compd. **797**, 612–621 (2019)
9. Han, J.J., Wang, C.P., Liu, X.J., et al.: Abnormal correlation between phase transformation and cooling rate for pure metals. Sci. Rep. **6**(1), 22391 (2016)
10. Wang, Y., Chen, X., Geng, H., et al.: Amorphization and crystallization of $Zr_{66.7-x}Cu_{33.3}Nb_x$ (x = 0, 2, 4) alloys during mechanical alloying. J. Alloys Comp. **474**(1–2):152–157 (2009)
11. Adelfar, R., Mirzadeh, H., Ataie. A., et al.: Amorphization and mechano-crystallization of high-energy ball milled Fe-Ti alloys. J. Non-Crystal. Solids. **520**:119466 (2019)
12. Yu, B.Y., Liang, Y.C., Tian, Z.A., Liu, R.S., Gao, T.H., Xie, Q., MoY.F.: MD simulation on crystallization mechanisms of rapidly supercooled Fe-Ni alloys. J. Cryst. Growth. **535**
13. Cui, Z., Bai, K., Wang, X., Li, E., Zheng, J.S: Electronic, magnetism, and optical properties of transition metals adsorbed g-GaN. Physica E: Low-dimension Syst Nanostruct. **118** (2020)
14. Cui, Z., Wang, M.J., Lyu, N., Zhang, S., Ding, Y.C., Bai, K.: Electronic, magnetism and optical properties of transition metals adsorbed puckered arsenene. Superlattices Microstruct. **152** (prepublish):106852 (2021)
15. Brown, W.M., Kohlmeyer, A., Plimpton, S.J., Tharrington, A.N.: Implementing molecular dynamics on hybrid high performance computers-particle-particle particle-mesh. Comput. Phys. Commun. **183**, 449–459 (2012)
16. Martyna, G.J., Tobias, D.J., Klein, M.L.: Constant pressure molecular dynamics algorithms. J. Chem. Phys. **101**(5), 4177–4189 (1994)
17. Pun, G.P., Mishin, Y.: "Embedded-atom potential for hcp and fcc cobalt," Phys. Rev. B. **86** 134116 (2012).
18. Kerimov, Elshat, Yu, et al.: Isothermal sections of the Co-Ni-Ta phase diagram at 1200 and 1375 K. J. Alloys Comp.: An Interdisciplin. J. Mater. Sci. Solid-State Chem. Physic (2017)
19. Haile, J.M., Johnston, I., Mallinckrodt, A.J., et al.: Molecular dynamics simulation: elementary methods. Am. Inst. Phys (1993)
20. Tian, Z.A., Liu, R.S., Dong, K.J., Yu, A.B.: A new method for analyzing the local structures of disordered systems. EPL **96**, 36001 (2011)
21. Stukowski, A.: Visualization and analysis of atomistic simulation data with OVITO–the Open Visualization Tool. Model. Simul. Mater. Sci. Eng. **18**, 2154–2162 (2010)
22. Qi, Y., et al.: Melting and crystallization in Ni nanoclusters: the mesoscale regime. J. Chem. Phys. **115**(1), 385–394 (2001)
23. Dana, J., Honeycutt, H., et al.: Molecular dynamics study of melting and freezing of small Lennard-Jones clusters. J. Physic. Chem. **91** (1987)
24. Pengju, Pan, Bo, et al.: Effect of crystallization temperature on crystal modifications and crystallization kinetics of poly(L-lactide). J. Appl. Polym. Sci. **107**(1):54–62 (2008)
25. Debenedetti, P.G., Stillinger, F.H.: Supercooled liquids and the glass transition. Nat. **410**, 259–267 (2001)
26. Frank, F.C., Kasper, J.S.: Complex alloy structures regarded as sphere packings. I. Definitions and basic principles. Acta Cryst. **11**:184–190 (1958)
27. Wang, Y.Y., Yu, P., Zhang, T., et al.: Microstructural evolution and densification of $Fe_{80}P_{11}C_9$ metallic glass under high pressure. Mater Sci Tech-Lond. **30**(14), 1774–1777 (2014)
28. Hou, Z.Y., et al.: Three-dimensional topological structures and formation processes of dislocations in Au nanowire under tension loading. Comput. Mater. Sci. **197** (2021)
29. Abbasfard, H., Evans, G., Moreno-Atanasio, R.: Effect of van der Waals force cut-off distance on adhesive collision parameters in DEM simulation. Powder Technol. **299**, 9–18 (2016)
30. Baer, S.: Structure and entropy change in amorphous materials. J. Non-Crystalline Solids. **117**(part-P1):183–186 (1990)
31. Tian, Z.A., Zhou, L.L., Mo, Y.F., Liang, Y.C., Liu, R.S.: Cooling rate dependence of polymorph selection during rapid solidification of liquid metal zinc. Trans. Nonferrous Met. Soc. China **25**(12), 4072–4079 (2015)
32. Liang, Y.C., et al.: Icosahedron-forming ability of Mg-Zn alloys studied by molecular dynamics simulations. J. Alloys Comp. (2017)
33. Ran, C.Y., Zhou, L.L., Liang, Y.C., et al.: Study on Si-like and topologically close-packed structures during rapid solidification of Au-Si alloys. J. Non-Crystalline Solids. **563**:120787 (2021)